Chirality-Induced Spin-Polarized State of a Chiral Crystal $CrNb_3S_6$

Akito Inui,[1] Ryuya Aoki,[1] Yuki Nishiue,[1] Kohei Shiota,[1] Yusuke Kousaka,[1] Hiroaki Shishido,[1] Daichi Hirobe,[2] Masayuki Suda,[2] Jun-ichiro Ohe,[3] Jun-ichiro Kishine,[2,4] Hiroshi M. Yamamoto,[2,*] and Yoshihiko Togawa[1,†]
[1]*Department of Physics and Electronics, Osaka Prefecture University, 1-1 Gakuencho, Sakai, Osaka 599-8531, Japan*
[2]*Research Center of Integrative Molecular Systems, Institute for Molecular Science, Okazaki, Aichi 444-8585, Japan*
[3]*Department of Physics, Toho University, Chiba 274-8510, Japan*
[4]*Division of Natural and Environmental Sciences, The Open University of Japan, Chiba, 261-8586, Japan*

(Received 1 March 2020; accepted 31 March 2020; published 21 April 2020)

Chirality-induced spin transport phenomena are investigated at room temperature without magnetic fields in a monoaxial chiral dichalcogenide $CrNb_3S_6$. We found that spin polarization occurs in these chiral bulk crystals under a charge current flowing along the principal c axis. Such phenomena are detected as an inverse spin Hall signal which is induced on the detection electrode that absorbs polarized spin from the chiral crystal. The inverse response is observed when applying the charge current into the detection electrode. The signal sign reverses in the device with the opposite chirality. Furthermore, the spin signals are found over micrometer length scales in a nonlocal configuration. Such a robust generation and protection of the spin-polarized state is discussed based on a one-dimensional model with an antisymmetric spin-orbit coupling.

DOI: 10.1103/PhysRevLett.124.166602

Introduction.—A connection between structural and dynamical chirality [1] can trigger a wide range of nontrivial physical responses. Indeed, a variety of chirality-driven phenomena such as optical rotation, magnetochiral dichroism [2], and nonreciprocal transport [3] have been found in various chiral systems including chiral liquid crystals [4], chiral helimagnets [5], chiral nanoelements [6], and chiral molecules [7].

Recently, it was found that chiral molecular systems exhibit chirality-induced spin selectivity (CISS) [8,9], as demonstrated by spin-polarized photocurrent emission [10] and tunneling transport [11,12] experiments. These observations indicate that chiral molecules emit a charge current which is spin polarized parallel or antiparallel to its flow direction depending on P or M chirality (right- or left-handed structure such as a helix) of the molecule, although the mechanism remains to be clarified. The CISS can be utilized in many multidisciplinary applications using chiral molecules such as electrochemistry [13], a self-assembled monolayer device [14], and enantioseparation [15]. However, the CISS is limited to interfacial phenomena, which prevent solid state device applications as well as a demonstration of the inverse phenomena. A realization of the CISS in a bulk material is useful in understanding the CISS mechanism. At the same time, a confirmation of the direct and inverse phenomena (reciprocity check) in such chiral bulk systems is indispensable in theoretical investigations.

In this Letter, chirality-induced transport properties are investigated in a monoaxial chiral dichalcogenide $CrNb_3S_6$. The experimental setup designed for the CISS detection using a chiral bulk crystal enables us to demonstrate that a charge current can induce spin-polarized carries in the chiral crystal by measuring an inverse spin Hall signal. In this experiment, the spin polarization can be reversed by switching the current direction as well as by changing the crystalline chirality of the device. The inverse CISS (ICISS) signal is also detected in the same device, which confirms the reciprocal relationship of the CISS phenomena. Surprisingly, the CISS signals are found over micrometer length scales in a nonlocal configuration, implying the existence of the spin-polarized state protected by the chiral crystalline structure. The generation and protection of the spin polarization over the whole chiral crystal is discussed based on a one-dimensional model taking into account an antisymmetric spin-orbit interaction (SOI) reflecting the material symmetry.

Crystal structure.—Bulk crystals of a monoaxial dichalcogenide $CrNb_3S_6$ [16] were grown using a chemical-vapor transport method, as described elsewhere [17]. It belongs to the space group $P6_322$ and, thus, has a left- or right-handed crystalline structure which consists of hexagonal planes of NbS_2 and intercalated Cr atoms, as illustrated in Fig. 1(a). The unit cell size is 0.57 nm in the ab plane and 1.21 nm along the c axis. The crystal growth of a pure enantiomorphic $CrNb_3S_6$ and the selection of the desired crystalline chirality [18] remain an open issue.

Device structure.—Let us explain the basic concept and device design for detecting spin polarization of a chiral crystal under a charge current. The device drawn in Fig. 1(b) was designed in order to validate the direct and inverse CISS effects in chiral crystals. We put a detection electrode on the chiral crystal which is presumed to be in a

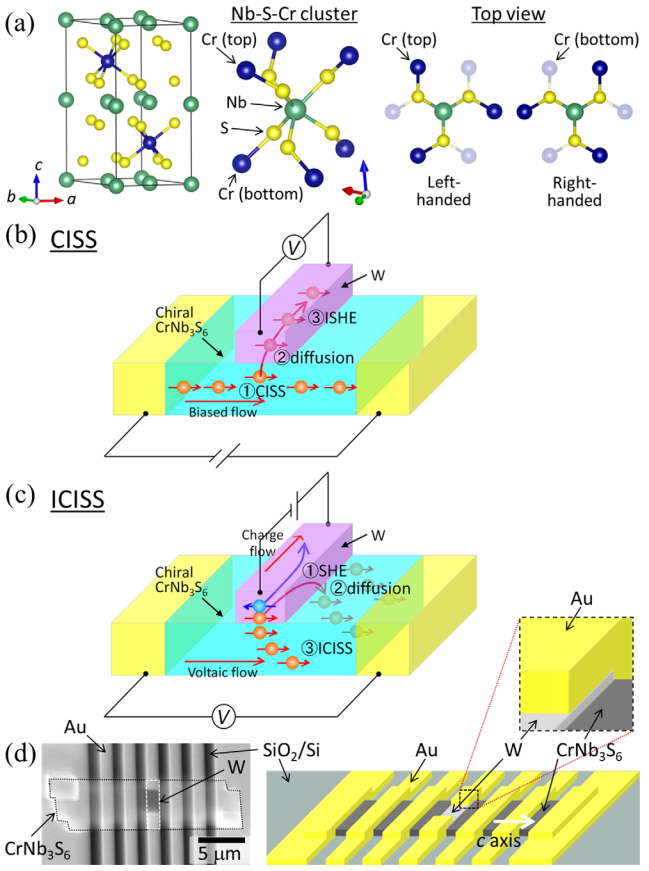

FIG. 1. Schematics of a crystal structure of $CrNb_3S_6$ (a) and device design (b),(c), together with a scanning electron micrograph (top view) of the device fabricated on a SiO_2/Si substrate (d). The device is made of a $CrNb_3S_6$ strip with a tungsten electrode at the center and gold electrodes beside. The c axis of $CrNb_3S_6$ is indicated by a white arrow. An enlarged image on the upper right in (d) shows the area of the tungsten electrode edge, which is partially covered by the gold electrode.

spin-polarized state owing to the charge current flowing along the c axis. The electrode is made of tungsten, which has a large spin Hall angle [19,20] so as to convert the spin polarization into the charge current via the inverse spin Hall effect (ISHE) [21–23]. This corresponds to the direct CISS detection, as schematically presented in Fig. 1(b).

The inverse CISS phenomena should be detectable in the same device, as shown in Fig. 1(c). When applying the charge current into the detection electrode, the spin current is injected into the chiral crystal beneath the electrode via the spin Hall effect (SHE) [23]. If the ICISS effect exists, the charge current should be generated in the chiral crystal.

For device fabrication, micrometer-sized strip samples were prepared from the bulk single crystal using focused ion beam methods in the same way as described in Ref. [5]. A typical device fabricated on a thermally oxidized silicon substrate is shown in Fig. 1(d). The $CrNb_3S_6$ sample size is 16.1 μm × 3.9 μm × 0.3 μm, where the longest dimension is parallel to the c axis. The samples have a tapered structure toward the edges along the width direction to have a good electrical contact. A tungsten detection electrode was fabricated on the sample center by using electron beam lithography and lift-off techniques. In this study, three devices were made for the CISS and ICISS detections. The thicknesses of the detection electrode are 6, 9, and 20 nm for three devices, labeled as device 1, 2, and 3, respectively, while the width is fixed to be 1 μm for all the devices. The resistivity values of $CrNb_3S_6$ and tungsten were evaluated to be 650 and 230 $\mu\Omega$ cm, respectively. In addition, gold electrodes (200 nm in thickness, 1 μm in width and gap) are made beside the tungsten electrode together with the current injection electrodes at both edges of the strip.

This configuration of electrodes in the device is useful for performing nonreciprocal electrical magnetochiral (EMC) transport measurements [5]. The EMC signals can provide information on the crystalline chirality of the device and its distribution inside the device, since the sign of the EMC coefficient $\hat{\gamma}$ reflects the crystalline chirality of the detection region between the electrodes, as demonstrated in Figs. 2 and 3. Furthermore, nonlocal signal detection can be performed in this device, as seen in Fig. 3.

The EMC coefficient $\hat{\gamma}$, which was obtained from the slope of the EMC signal in Fig. 2(a) [5], was evaluated to be -3.4×10^{-15}, -2.4×10^{-15}, and 9.4×10^{-16} $m^2\,T^{-1}\,A^{-1}$ at 150 K for devices 1, 2, and 3, respectively. It is clear that device 3 has the handedness opposite to those for the other devices (1 and 2) around the center region of the device.

Measurement method.—All the electrical transport measurements are performed at room temperature in this study. The induced voltages are examined as a function of the current with no magnetic field. Note that $CrNb_3S_6$ exhibits a helimagnetic phase transition below the critical temperature T_c of about 130 K [24]. However, at temperatures far above T_c, the electrical transport signals should be free from the contribution of chiral magnetic order, which is formed below T_c. Spin fluctuations, being prominent around T_c, are also expected to be very weak at room temperature, as demonstrated by the electrical EMC transport experiments with $CrNb_3S_6$ [5].

For the direct CISS detection, the current is applied in the direction along the c axis of $CrNb_3S_6$, and the transverse voltage is measured in the tungsten detection electrode. The current was swept between ±1 mA, the amplitude of which corresponds to a current density of 8.6×10^8 A/m^2 in the case of device 2. The Joule heating effect is negligibly small at this value.

On the other hand, for the ICISS detection, the current is applied into the tungsten electrode, and the generated voltage is monitored between the electrodes at both strip edges of $CrNb_3S_6$. The current was altered between ±10 μA.

Direct and inverse CISS measurements.—The voltage signals were clearly found across the tungsten electrode and $CrNb_3S_6$ crystal in the direct and inverse measurements, as

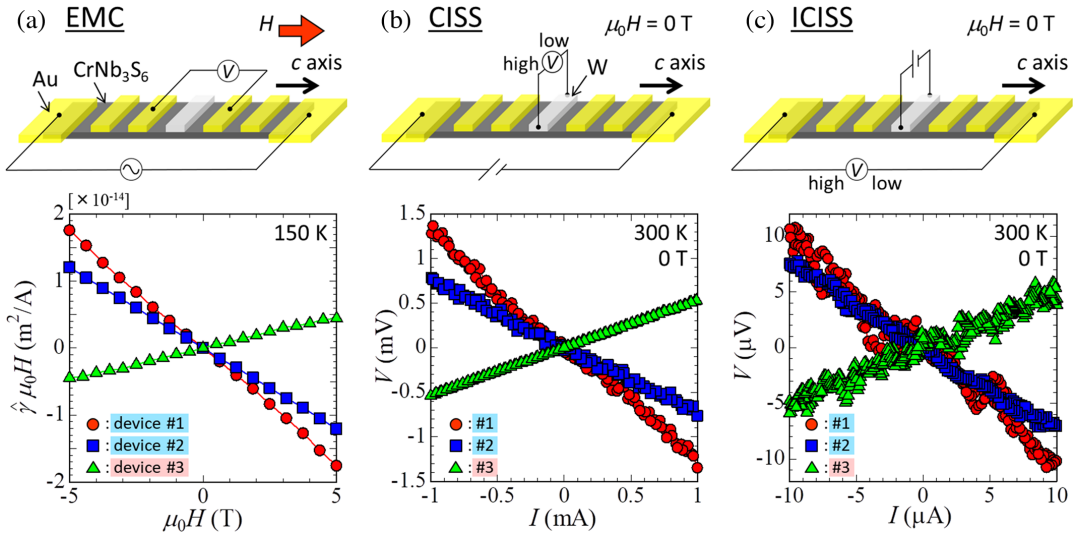

FIG. 2. A dataset and experimental setup of the EMC (a), direct CISS (b), and inverse CISS (c) measurements performed in the three $CrNb_3S_6$ devices with the tungsten electrode. The EMC signals taken at 150 K with sweeping the magnetic field are given in the normalized unit (m^2/A) to see the EMC coefficient $\hat{\gamma}$ in (a). Current-voltage CISS and ICISS characteristics at 300 K at 0 T are provided in (b) and (c), respectively. The slope values of the CISS and ICISS signals are −1.35 and −1.05 Ω for device 1, −0.77 and −0.76 Ω for 2, and 0.54 and 0.49 Ω for 3, respectively.

shown in Figs. 2(b) and 2(c), respectively. The signal changes linearly with a negative slope from a negative to positive current regime for devices 1 and 2. On the other hand, device 3, which has the opposite handedness,

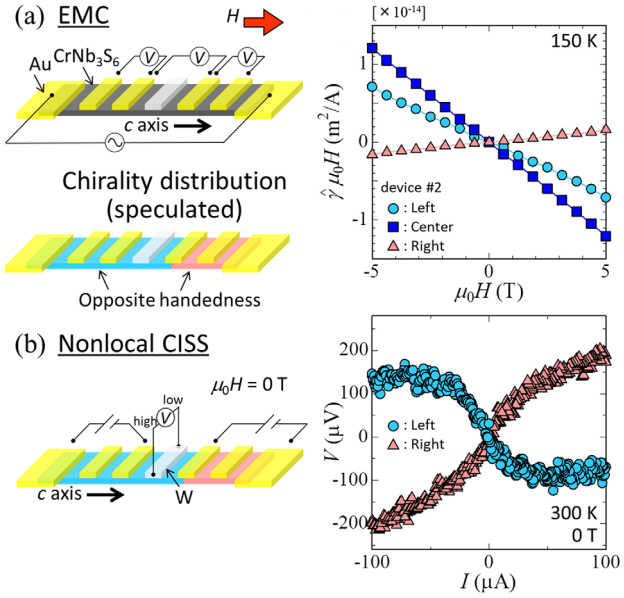

FIG. 3. A dataset and experimental setup of the EMC (a) and nonlocal CISS (b) measurements. The chirality distribution was examined by using the EMC data in the left, center, and right areas of device 2. The data for the center area are the same ones shown in Fig. 2(a). The nonlocal CISS data were obtained with a configuration where the current was injected in the left and right areas of the device. The slope values of the nonlocal CISS signal are −4.36 and 4.24 Ω in the linear regime at a small current, respectively.

exhibits a positive slope in the linear voltage response in both measurements. Namely, the signal sign becomes opposite in the devices with different chirality.

The slope values, summarized in the figure caption of Fig. 2, are almost the same between the direct and inverse measurements in all the devices. Interestingly, the absolute value of the slope increases with decreasing the thickness of the tungsten electrode, which could arise from the shunting effect of the electrode as well as chirality purity of the sample.

The transverse voltage may arise from longitudinal electrical resistance caused by a misalignment of gold electrodes attached to the tungsten electrode. If the obtained signal is completely due to the misalignment, it would reach 340 nm, taking into account a longitudinal resistance value of $CrNb_3S_6$ (4 Ω/μm for device 1). However, it is hard to see such a large misalignment of the electrodes in the picture of the device in Fig. 1(d). Furthermore, in a separate experiment using the device with the same configuration of electrodes but with no tungsten detection electrode, the longitudinal component in the conventional Hall voltage was evaluated to occur due to the misalignment of 30 nm at a maximum. Such artifacts hardly explain the signal intensity observed in the present device, indicating that the intrinsic mechanism is required to induce it.

These experimental results strongly support that the direct and inverse CISS effects work in the chiral crystals. Namely, moving electrons in the chiral crystal becomes spin polarized parallel or antiparallel to the flow direction of the applied charge current, while the spin-polarized state induced in the chiral crystal generates the charge flow spontaneously. It is notable that the reversal of the current

direction generates spin polarization in the opposite direction, which is also consistent with the CISS symmetry. The sign reversal of the signal against the chirality reversal of the crystal, which is also a typical CISS response, is successfully confirmed as well.

We stress that the sign of the CISS and ICISS signals is well correlated with that of the EMC signal. Namely, the CISS detection can be a counterpart for identifying the crystalline chirality of chiral inorganic crystals or chiral bulk materials. As for the intensity, the correlation is likely to hold among them. However, careful study using devices with opposite handedness and the detection electrode of the same thickness is required to clarify the relationship of the signal intensity.

Nonlocal CISS measurement.—It is interesting to examine how the spin-polarized state due to the CISS effect distributes over the chiral crystal. For this purpose, the CISS detection was performed in a nonlocal transport setup using the same devices. The charge current is applied between the gold electrodes in the left or right side of the device where the tungsten detection electrode is not included. Then, the nonlocal signal is measured on the tungsten electrode in order to see whether or not the spin polarization of $CrNb_3S_6$ survives in a distant area where no charge current flows. The EMC signal was also examined in each area for the chirality identification.

Figure 3(a) shows the location-dependent EMC data of device 2. It turns out that the right area has a chirality different from that of the left side. Note that the center area has the same chirality as the left side. Figure 3(b) exhibits the CISS data obtained in a nonlocal configuration on the left and right sides. The signal appears at the tungsten electrode, being located more than one micrometer away from the areas where the current is injected. A linear response is found at the small current regime, while the signal reduces the slope value or is likely to be saturated at the high current regime. Importantly, the signal sign is reversed in both cases, thus indicating that it is sensitive to the chirality of the area of the current injection.

The CISS signals detected in nonlocal measurements suggest that the spin-polarized state is locally generated by the charge current in the region where the current flows and such a spin polarization retains over micrometer length scales to reach the detection electrode. This requires a nontrivial physical picture of generating and protecting the CISS response in the chiral crystal.

Theoretical insight.—A possible mechanism underlying a robust generation and protection of the spin-polarized state in a monoaxial chiral crystal is discussed in terms of an electronic state of the chiral crystal. Because of monoaxial crystal symmetry without rotoinversion symmetry (hexagonal $P6_322$ space group), an electron one-particle process acquires an antisymmetric SOI of the form $\alpha_1(k_x\sigma_x + k_y\sigma_y) + \alpha_2 k_z\sigma_z$ [25]. This form of the antisymmetric SOI has the same origin as the Lifshitz invariant for the magnetic spins in the same crystal [26]. This correspondence indicates that the transverse component is negligible as compared with the longitudinal one, i.e., $|\alpha_1| \ll |\alpha_2|$. In such a case, the electron one-particle Hamiltonian along the z (principal c) axis becomes $H \simeq \hbar^2 k_z^2/2m + \alpha_2 k_z\sigma_z \simeq \hbar^2(k_z \pm m\alpha_2/\hbar^2)^2/2m$, where $+$ and $-$ signs, respectively, correspond to the spin right ($\rightarrow$ in the $+z$ direction) and left ($\leftarrow$ in the $-z$ direction).

In the region where the electric current flows, the CISS effect causes the chemical potential difference depending on the spin directions: $\mu_{\rightarrow}(z) \neq \mu_{\leftarrow}(z)$. The bias voltage causes the linear slope of the chemical potentials along the z axis. A combination of the spin directions at high and low levels in the chemical potential is altered depending on the chirality of the crystal as well as the direction of the charge flow.

The experimental findings in the nonlocal measurements indicate that this spin-dependent chemical potential difference is kept even in the region without the current flow. Namely, the difference is retained, because there is no spin-flipping process due to the monoaxial nature of the antisymmetric SOI. Then, the tungsten detection electrode plays a role of probing the spin-dependent chemical potential difference through the diffusive spin current extracted from the spin-polarized $CrNb_3S_6$.

Discussion and perspective.—In conventional materials, the spin polarization decays within a spin diffusion length in the nonlocal transport setup. It depends on the SOI strength and is as small as 500, 50, and 5 nm at 300 K for copper, gold, and permalloy, respectively [19]. Nevertheless, the nonlocal CISS response survives over one micrometer in the monoaxial chiral crystal $CrNb_3S_6$ even though it is in a category of materials subject to a strong SOI. Thus, the antisymmetric nature of the SOI should play a key role in triggering such a robust spin-polarized state in $CrNb_3S_6$.

Spin-momentum locking has attracted considerable interest in Rashba two-dimensional systems such as semiconductors [27] and topological materials [28], where spin orientation is constrained to be perpendicular to electron momentum. In our case, spin-momentum locking due to the antisymmetric SOI under monoaxial chiral (precisely Sohncke) symmetry results in a unique arrangement of spin momentum parallel to electron flow, which is in favor of an emergence of the robust CISS response.

Current-induced magnetization (bulk Edelstein effect) was recently reported in chiral tellurium bulk materials by means of nuclear magnetic resonance measurements [29]. Orbital and spin magnetic moments were theoretically evaluated for related compounds, and the former was regarded as a dominant term in the case of tellurium [30]. No direct detection of the spin momentum has been done yet, and distinguishing orbital and spin counterparts remains an important open issue.

The spin-dependent transport measurements performed in this study demonstrated that the CISS effect originally found in chiral molecules emerges in a chiral inorganic bulk

crystal. We believe that this finding sheds light on many essential issues in experimental and theoretical viewpoints. The CISS has been observed so far in a highly nonlinear situation [10] or tunneling transport regime [11,12] in a chiral molecular system. Our results clarified that the CISS and ICISS appear even in a linear response regime in chiral inorganic crystals, which will be an important clue for future theoretical works. For instance, the description based on a molecular orbital scheme should be connected to that with k-space band theory for a successful interpretation of the CISS phenomena. In application viewpoints, the robust CISS response in chiral bulk crystals may open up a novel route for spin manipulation in solid state devices. Furthermore, an electrical detection of the chirality via the CISS instead of the EMC is useful for a wide range of chiral materials. Advantages of such a method are found in various aspects: The experimental condition and procedure of the CISS measurement are much simpler than those for the EMC detection. The detection electrode can work as a local probe in a reduced dimension. Probing the chirality in a local area or monitoring a growth process of homochiral materials will be promising research targets.

We thank Yusuke Kato, Takuya Sato, and Alexander S. Ovchinnikov for useful discussions and a critical reading of the manuscript. We acknowledge support from Grants-in-Aid for Scientific Research (No. 17H02767, No. 17H02923, No. 19K03751 and No. 19H00891) and Research Grant of Specially Promoted Research Program by Toyota RIKEN. A part of this work was conducted in Equipment Development Center (Institute for Molecular Science), supported by Nanotechnology Platform Program (Molecule and Material Synthesis) of the Ministry of Education, Culture, Sport, Science and Technology (MEXT), Japan.

*yhiroshi@ims.ac.jp
†y-togawa@pe.osakafu-u.ac.jp

[1] L. Barron, *Molecular Light Scattering and Optical Activity* (Cambridge University Press, Cambridge, England, 1982).
[2] G. L. J. A. Rikken and E. Raupach, Observation of magneto-chiral dichroism, Nature (London) **390**, 493 (1997).
[3] G. L. J. A. Rikken, J. Fölling, and P. Wyder, Electrical Magnetochiral Anisotropy, Phys. Rev. Lett. **87**, 236602 (2001).
[4] *Chirality in Liquid Crystals*, edited by H.-S. Kitzerow and C. Bahr (Springer-Verlag, New York, 2001).
[5] R. Aoki, Y. Kousaka, and Y. Togawa, Anomalous Nonreciprocal Electrical Transport on Chiral Magnetic Order, Phys. Rev. Lett. **122**, 057206 (2019).
[6] H.-E. Lee, H.-Y. Ahn, J. Mun, Y. Y. Lee, M. Kim, N. H. Cho, K. Chang, W. S. Kim, J. Rho, and K. T. Nam, Amino-acid- and peptide-directed synthesis of chiral plasmonic gold nanoparticles, Nature (London) **556**, 360 (2018).
[7] F. Pop, P. Auban-Senzier, E. Canadell, G. L. J. A. Rikken, and N. Avarvari, Electrical magnetochiral anisotropy in a bulk chiral molecular conductor, Nat. Commun. **5**, 3757 (2014).
[8] R. Naaman and D. H. Waldeck, Chiral-induced spin selectivity effect, J. Phys. Chem. Lett. **3**, 2178 (2012).
[9] R. Naaman and D. H. Waldeck, Spintronics and chirality: Spin selectivity in electron transport through chiral molecules, Annu. Rev. Phys. Chem. **66**, 263 (2015).
[10] B. Göhler, V. Hamelbeck, T. Z. Markus, M. Kettner, G. F. Hanne, Z. Vager, R. Naaman, and H. Zacharias, Spin selectivity in electron transmission through self-assembled monolayers of double-stranded DNA, Science **331**, 894 (2011).
[11] Z. Xie, T. Z. Markus, S. R. Cohen, Z. Vager, R. Gutierrez, and R. Naaman, Spin specific electron conduction through DNA oligomers, Nano Lett. **11**, 4652 (2011).
[12] M. Suda, Y. Thathong, V. Promarak, H. Kojima, M. Nakamura, T. Shiraogawa, M. Ehara, and H. M. Yamamoto, Light-driven molecular switch for reconfigurable spin filters, Nat. Commun. **10**, 2455 (2019).
[13] M. Kettner, B. Göhler, H. Zacharias, D. Mishra, V. Kiran, R. Naaman, C. Fontanesi, D. H. Waldeck, S. Sęk, J. Pawłowski, and J. Juhaniewicz, Spin filtering in electron transport through chiral oligopeptides, J. Phys. Chem. C **119**, 14542 (2015).
[14] K. S. Kumar, N. Kantor-Uriel, S. P. Mathew, R. Guliamova, and R. Naaman, A device for measuring spin selectivity in electron transfer, Phys. Chem. Chem. Phys. **15**, 18357 (2013).
[15] K. Banerjee-Ghosh, O. B. Dor, F. Tassinari, E. Capua, S. Yochelis, A. Capua, S.-H. Yang, S. S. P. Parkin, S. Sarkar, L. Kronik, L. T. Baczewski, R. Naaman, and Y. Paltiel, Separation of enantiomers by their enantiospecific interaction with achiral magnetic substrates, Science **360**, 1331 (2018).
[16] Y. Togawa, Y. Kousaka, K. Inoue, and J. Kishine, Symmetry, structure, and dynamics of monoaxial chiral magnets, J. Phys. Soc. Jpn. **85**, 112001 (2016).
[17] Y. Kousaka, Y. Nakao, J. Kishine, M. Akita, K. Inoue, and J. Akimitsu, Chiral helimagnetism in $T_{1/3}NbS_2$ (T = Cr and Mn), Nucl. Instrm. Methods Phys. Res., Sect. A **600**, 250 (2009).
[18] Y. Kousaka, T. Koyama, K. Ohishi, K. Kakurai, V. Hutanu, H. Ohsumi, T. Arima, A. Tokuda, M. Suzuki, N. Kawamura, A. Nakao, T. Hanashima, J. Suzuki, J. Campo, Y. Miyamoto, A. Sera, K. Inoue, and J. Akimitsu, Monochiral helimagnetism in homochiral crystals of $CsCuCl_3$, Phys. Rev. Mater. **1**, 071402 (2017).
[19] H. L. Wang, C. H. Du, Y. Pu, R. Adur, P. C. Hammel, and F. Y. Yang, Scaling of Spin Hall Angle in 3d, 4d, and 5d Metals from $Y_3Fe_5O_{12}$/Metal Spin Pumping, Phys. Rev. Lett. **112**, 197201 (2014).
[20] Y. Niimi and Y. Otani, Reciprocal spin Hall effects in conductors with strong spinorbit coupling: A review, Rep. Prog. Phys. **78**, 124501 (2015).
[21] S. O. Valenzuela and M. Tinkham, Direct electronic measurement of the spin Hall effect, Nature (London) **442**, 176 (2006).
[22] E. Saitoh, M. Ueda, H. Miyajima, and G. Tatara, Conversion of spin current into charge current at room temperature: Inverse spin-Hall effect, Appl. Phys. Lett. **88**, 182509 (2006).

[23] T. Kimura, Y. Otani, T. Sato, S. Takahashi, and S. Maekawa, Room-Temperature Reversible Spin Hall Effect, Phys. Rev. Lett. **98**, 156601 (2007).

[24] Y. Togawa, T. Koyama, K. Takayanagi, S. Mori, Y. Kousaka, J. Akimitsu, S. Nishihara, K. Inoue, A. S. Ovchinnikov, and J. Kishine, Chiral Magnetic Soliton Lattice on a Chiral Helimagnet, Phys. Rev. Lett. **108**, 107202 (2012).

[25] P. A. Frigeri, Superconductivity in crystals without an inversion center, Ph.D. thesis, ETH-Zürich, 2005.

[26] J. Kishine and A. S. Ovchinnikov, Theory of monoaxial chiral helimagnet, Solid State Phys. **66**, 1 (2015).

[27] M. Kohda, T. Okayasu, and J. Nitta, Spin-momentum locked spin manipulation in a two-dimensional Rashba system, Sci. Rep. **9**, 1909 (2019).

[28] Y. Shiomi, K. Nomura, Y. Kajiwara, K. Eto, M. Novak, K. Segawa, Y. Ando, and E. Saitoh, Spin-Electricity Conversion Induced by Spin Injection into Topological Insulators, Phys. Rev. Lett. **113**, 196601 (2014).

[29] T. Furukawa, Y. Shimokawa, K. Kobayashi, and T. Itou, Observation of current-induced bulk magnetization in elemental tellurium, Nat. Commun. **8**, 954 (2017).

[30] T. Yoda, T. Yokoyama, and S. Murakami, Current-induced orbital and spin magnetizations in crystals with helical structure, Sci. Rep. **5**, 12024 (2015).